PROPOSAL FOR IASI ON-BOARD DATA COMPRESSION

Joaquín García-Sobrino[a], Ian Blanes[a], Mathieu Albinet[b], Roberto Camarero[b], and Joan Serra-Sagristà[a]

[a]Dept. of Information and Communications Engineering
Universitat Autònoma de Barcelona
Edifici Q, UAB, E-08193 Cerdanyola del Vallès (Barcelona), Spain
Email: joaquin.garcia.sobrino@deic.uab.es, {ian.blanes, joan.serra}@uab.cat
[b]Centre national d'études spatiales
CNES, 18 av. Edouard Belin, 31401 Toulouse Cedex 9, France
Email: {mathieu.albinet, roberto.camarero}@cnes.fr

The Infrared Atmospheric Sounding Interferometer (IASI) system provides infrared soundings of moisture and temperature profiles, as well as soundings of chemical components. These measurements play a key role in atmospheric chemistry, global change and climate monitoring. The instrument, developed by a cooperating agreement between EUMETSAT and CNES, is implemented on the Metop satellite series.

The instrument data production rate is 45 Megabits/s while the transmission rate allocated to IASI measurements is 1.5 Megabits/s. It is thus necessary to implement a significant part of the IASI data processing on board the instrument.

In this paper we investigate the information statistics of IASI L0 data once the on-board processing chain is finished. We analyze order-0 entropy, and order-1, order-2 and order-3 conditional entropies, where conditional entropies assess both the spectral and the spatial joint information. According to the simple order-0 entropy, at least one bit per sample could be spared if a variable-length code were employed.

We also investigate the actual performance of different lossless compression techniques on IASI L0 data. The CCSDS-123, JPEG-LS and JPEG2000 standards, as well as M-CALIC coding technique are evaluated. Experimental results reveal that IASI Level 0 data can be coded by a compression ratio above 2.6:1.

Keywords: *remote sensing compression, lossless data coding, predictive coding, entropy analysis, multi- and hyperspectral imagery, CCSDS 123.*

1 Introduction

IASI is an Infrared Atmospheric Sounder Interferometer that provides atmospheric spectra to the scientific and meteorological communities. It is a key element of the payload on the Metop series of European meteorological polar-orbiting satellites. IASI represents a significant scientific and technological step forward that provides meteorologists with atmospheric emission spectra to derive temperature and humidity profiles with a vertical resolution of one kilometer and an accuracy of within one kelvin for temperature and 10% precision for humidity measurements [1].

IASI instrument scans the Earth surface in step and stare mode, harvesting atmospheric soundings on both sides of the vertical line, producing *fields of view* (FOV). Each FOV consists of four full spectra, where each spectrum represents a single circular pixel of the scanned image [2], [3]; all pixels are captured in the same way. Complete coverage of the Earth orbit is carried out by scanning lines at regular intervals. Each scanned line consists of thirty FOVs. Fig. 1a, reproduced from [4], shows the modus operandi of the IASI instrument. Each scanned pixel represents twelve kilometers of the Earth surface [3]. Pixels are spaced by approximately 12 kilometers, so that each FOV represents nearly fifty kilometers of the Earth surface at nadir position. Fig. 1b shows the structure and the pixel numbering of a FOV [5], while Fig. 1c reports the size of the Earth surface scanned by a FOV.

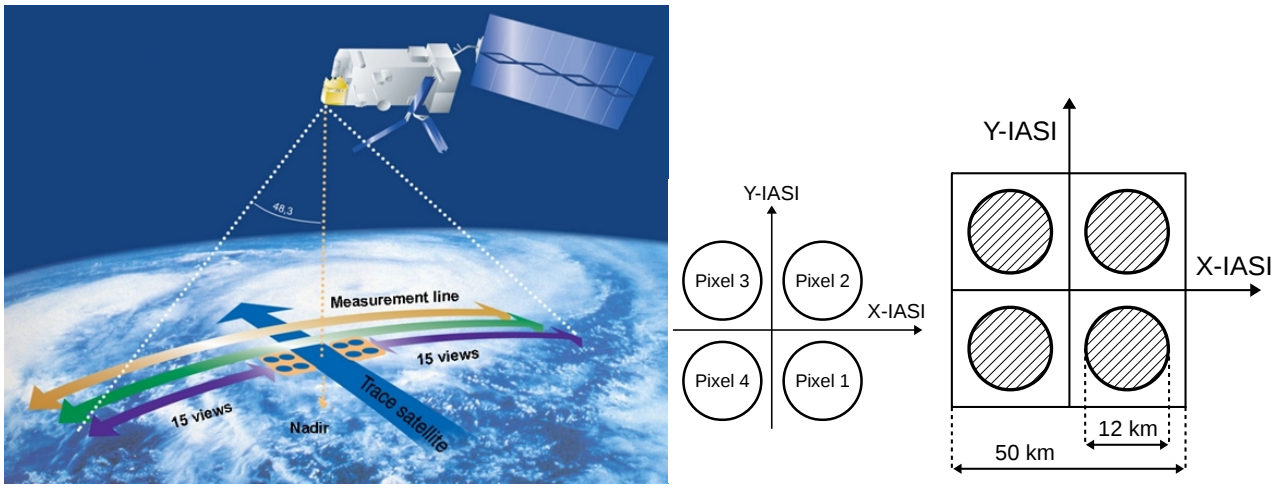

(a) Modus operandi of IASI instrument. (b) FOV pixel numbering (c) FOV size and pixel size

Figure 1: Details of the IASI instrument.

The IASI instrument provides infrared spectra with high resolution between wavelengths 645 cm^{-1} and 2760 cm^{-1}. The spectral resolution required from IASI after apodisation is equal to 0.5 cm^{-1}, i.e. 0.25 cm^{-1} before apodisation. This represents a challenge because today technology does not produce detectors having the required performance. It is necessary to implement three different detectors per pixel –providing three different sub-bands (B1, B2 and B3)– to supply the required spectral range [2]. The nominal limits of each sub-band are reported in Fig. 2a. However, this approach produces high noise level in sub-band edges, as shown in Fig. 2b, reproduced from [2], which leads to a band merging process to reduce the increased noise. This way, edges on sub-bands B1/B2 and B2/B3 are combined, resulting in a spectra less noisy than the original, but keeping the required spectral resolution (645 cm^{-1} to 2760 cm^{-1}).

While the IASI data production rate is 45 Megabits/s, the transmission rate allocated to these instrument measurements is 1.5 Megabits/s [6]. Accordingly, it is necessary to implement a significant part of the IASI data processing on board the instrument. An inverse Fourier transform and a radiometric calibration are performed on-board to reduce the size of the data to be transmitted. The spectral data are then encoded before being sent to the reception stations. This part of the IASI processing chain is known as Level 0.

8359 different spectral bands are captured for each pixel, producing 8359 samples. These samples are *splitted* into 522 ranges of 16 bands each one and 1 range of 7 bands (the last one). Each sample is quantized then coded as a natural number using a fixed amount of bits (from 6 to 10 bits, depending on the range) before its transmission to ground. The amount of bits for each sample was chosen to respect the NedT (Noise Equivalent Delta Temperature) degradation specification. In the end, spectral data are transmitted in the form of a bit-stream.

This method provides simplicity and a fixed bit-rate output, but presents risks of overflow and its performance is suboptimal. This choice was implemented in the instrument because most of the processing power in the dedicated electronic unit was devoted to perform the Fourier Transform.

The different processes performed on-board the satellite are described in Tournier et al. [6], where mathematical and

B1: from 645 cm^{-1} to 1210 cm^{-1}
B2: from 1210 cm^{-1} to 1900 cm^{-1}
B1: from 1900 cm^{-1} to 2760 cm^{-1}

(a) Nominal limits of sub-bands

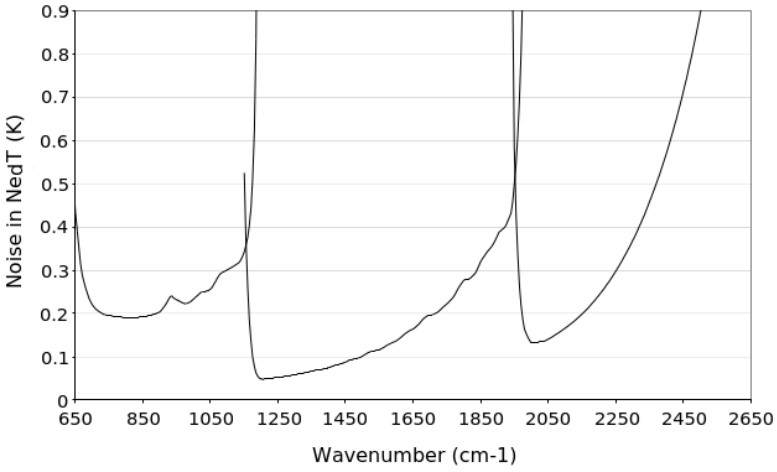

(b) Level noise in sub-bands

Figure 2: Sub-bands in IASI spectral range.

physical content of the IASI Level 0 processing algorithms are detailed. Different algorithms are run in real-time in order to complete the on-board processing chain [2].

Currently, the IASI instrument is able to transmit an average of 8.2 bits per spectral sample without loss of useful information [6]. However, information statistics of IASI L0 data once the on-board processing chain is finished suggests that a smaller amount of bits per spectral sample might be needed in practice.

IASI L0 data are not considered as end-user data and therefore they are not publicly available. To the best of our knowledge, no compression study beyond those related to the design of the instrument has been carried out.

This paper investigates the modification of the level 0 processing chain such that improved data transmission rate could be provided. We analyze the information statistics of IASI L0 data before being sent to ground. We study order-0 entropy, and order-1, order-2 and order-3 conditional entropies, where conditional entropies assess both the spectral and the spatial joint information. According to the studied contextual models, theoretical results suggest that between one and seven bits per sample might be spared if a variable-length code were employed.

The rest of the paper is organized as follows: Section 2 presents theoretical results about different order-n entropies for two sets of IASI L0 images. Section 3 presents experimental results of IASI L0 data compression using different techniques: CCSDS-123, JPEG-LS and JPEG2000 standards, and M-CALIC coding technique. Section 4 concludes the paper.

2 Entropy analysis on IASI L0 data

The information statistics analysis is performed on a corpus of sixteen 3D images consisting of a set of eight images from EUMETSAT and a set of eight images from CNES. Since raw data produced by the instrument are not available on ground, all the analyzed images are mounted using spectral data once the on-board processing chain is finished. All volumes are mounted using data sent from satellite to reception station before any further processing on ground. Table 1

provides the technical names of the employed IASI L0 products along with their identifier (id.) used in the remainder of the paper.

All IASI L0 images have 8359 bands, 60 columns and a different number of rows. Images from EUMETSAT have 172, 158, 110, 180, 196, 154, 110 and 132 rows, respectively. Images from CNES have a larger number of rows than images from EUMETSAT, with, respectively, 1484, 1484, 1528, 1482, 1528, 1528, 1528 and 1528 rows; this amount of rows approximates a full Earth orbit (1530 rows).

As explained, the on-board processing chain encodes each sample using a fix amount of bits, from 6 to 10 bits depending on the range, i.e., all samples belonging to a given range – and, thus, all samples from the same spectral component– are encoded using the same number of bits.

The entropy analysis presented in this paper comprises order-0 entropy, order-1 conditional entropy, order-2 conditional entropy and order-3 conditional entropy. Order-0 entropy is computed as described in Eq. (1), where $p(x)$ represents the probability of occurrence of symbol x.

$$H(X) = -\sum_{x \in X} p(x) \log_2 p(x) \tag{1}$$

The conditional entropy assesses the spatial and/or spectral joint information. Equation (2) provides the definition for order-1 conditional entropy. Order-2 conditional entropy and order-3 conditional entropy are defined accordingly.

$$H(X|Y) = -\sum_{x \in X, y \in Y} p(x,y) \log_2 \frac{p(x,y)}{p(y)} \tag{2}$$

Figure 3 illustrates the different contexts analyzed in the study. Order-0 entropy computes the statistics of the current pixel (Fig. 3a). Six different contextual models are taken into consideration for order-1 conditional entropy: the left pixel

Table 1: Analyzed images.

Id.	IASI L0 Product
EUMETSAT 1	IASI_HRP_00_M01_20130813184200Z_20130813185335Z_N_O_20130813184205Z
EUMETSAT 2	IASI_HRP_00_M01_20130813202226Z_20130813203309Z_N_O_20130813202229Z
EUMETSAT 3	IASI_HRP_00_M01_20130814070242Z_20130814071311Z_N_O_20130814070245Z
EUMETSAT 4	IASI_HRP_00_M01_20130814084228Z_20130814085440Z_N_O_20130814084231Z
EUMETSAT 5	IASI_HRP_00_M01_20130814101020Z_20130814102504Z_N_O_20130814101026Z
EUMETSAT 6	IASI_HRP_00_M01_20130814120024Z_20130814121046Z_N_O_20130814120030Z
EUMETSAT 7	IASI_HRP_00_M02_20130813192744Z_20130813193516Z_N_O_20130813192748Z
EUMETSAT 8	IASI_HRP_00_M02_20130814092926Z_20130814093921Z_N_O_20130814092930Z
CNES 1	IASI_xxx_00_M02_20091007112100Z_20091007130000Z_N_O_20091007125723Z
CNES 2	IASI_xxx_00_M02_20091007130000Z_20091007143900Z_N_O_20091007143543Z
CNES 3	IASI_xxx_00_M02_20091007143900Z_20091007162100Z_N_O_20091007161509Z
CNES 4	IASI_xxx_00_M02_20091017125400Z_20091017143300Z_N_O_20091017142943Z
CNES 5	IASI_xxx_00_M02_20100319050300Z_20100319064500Z_N_O_20100319064052Z
CNES 6	IASI_xxx_00_M02_20120718075700Z_20120718093900Z_N_O_20120718084400Z
CNES 7	IASI_xxx_00_M02_20130116133300Z_20130116151500Z_N_O_20130116142103Z
CNES 8	IASI_xxx_00_M02_20130916080300Z_20130916094500Z_N_O_20130916093859Z

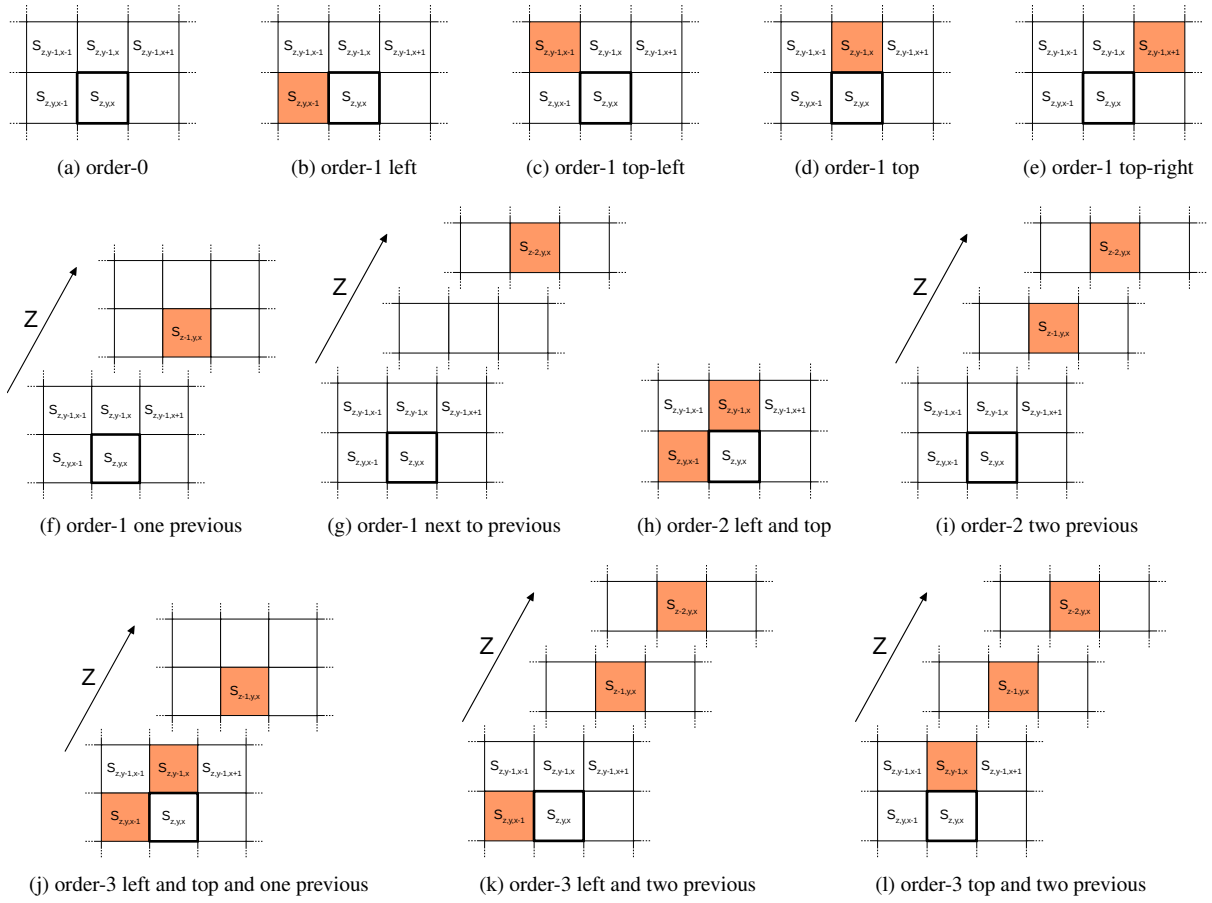

Figure 3: Defined contexts in the context-based entropy analysis.

(Fig. 3b), the top-left pixel (Fig. 3c), the top pixel (Fig. 3d), the top-right pixel (Fig. 3e), the co-located pixel in a previous component (Fig. 3f) and the co-located pixel in the next to previous component (Fig. 3g) are used as contexts. In the case of order-2 conditional entropy, two different contexts are considered, the left and the top pixel (Fig. 3h) and the co-located pixels in the previous and in the next to previous component (Fig. 3i). Three different order-3 conditional entropies are also investigated: the left, the top and the co-located pixel in a previous component (Fig. 3j); the left and the co-located pixels in the two previous components (Fig. 3k); and the top and the co-located pixels in the two previous components (Fig. 3l).

To get consistent results, only pixels having all the required contexts shall be analyzed. In this way, the first row and the first and the last column in a component are not considered for entropy computation, as their pixels lack some neighboring context. Regarding to spectral dependencies, only the last fourteen components in each range are analyzed, again because of some lacking neighboring contexts for the first two components.

Fig. 4 provides an example of the entropy distribution for a single range (range 11) for two of the analyzed volumes (EUMETSAT 1 and CNES 1). Range 11 comprises bands from 161 to 176 (both included), with all components coded with 9 bits per pixel (bpp). Columns in the graph correspond to different order-n entropies (contexts). Marks in columns represent the entropy of a single component. As explained, only fourteen marks per column are plotted.

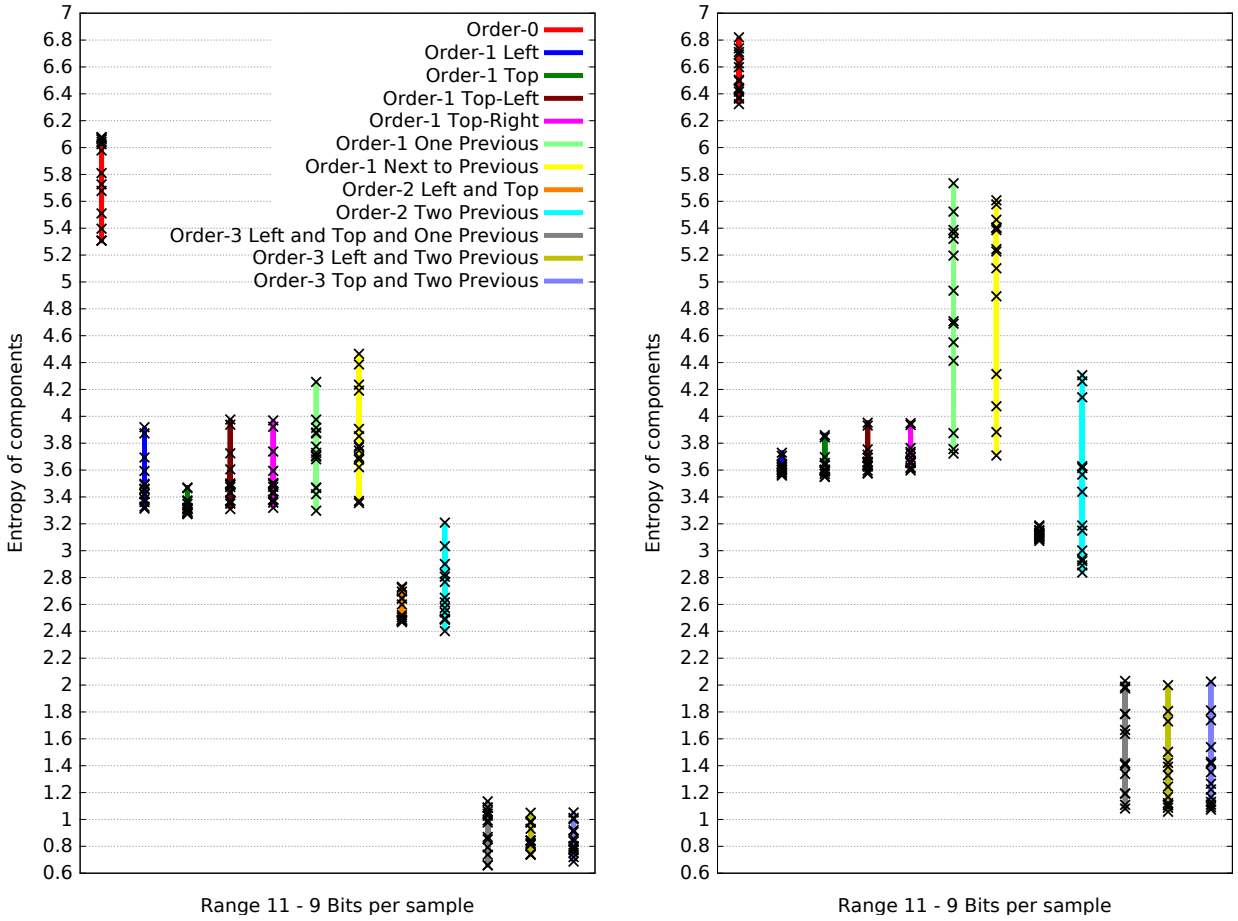

(a) EUMETSAT 1

(b) CNES 1

Figure 4: Entropy distribution of range 11 in bits per pixel (bpp). It is originally encoded with 9 bpp.

Because of space constraints, only plots corresponding to two images are reported. This same analysis is performed for all ranges (523) for each of the 16 images (EUMETSAT and CNES). Results indicate that the entropy distribution follows a very similar pattern in each range in all images. This behavior is common to images from both EUMETSAT and CNES corpus, the latter having a much larger number of rows. Even though the particular entropy values may differ, the entropy distribution of the different studied contexts is very similar, suggesting that the performance of the selected contextual model is similar for all IASI L0 data.

Table 2 and Table 3 report the results of the entropy analysis in the studied images. The different *entropy* columns provide the average entropy for all components in an image. Entropy is computed on a per component basis. The average entropy is calculated to determine the theoretical average number of bits per pixel needed to encode the whole image.

Currently, the on-board processing chain implemented in the instrument allows to encode the IASI L0 data using, on average, 8.2 bpp before being transmitted to reception stations. The theoretical order-0 entropy analysis yields that images from EUMETSAT and CNES could be coded using, on average, 5.96 bpp and 6.35 bpp, respectively. This implies that 2.23 bpp and 1.84 bpp might be spared in images from EUMETSAT and CNES, respectively, if a simple variable-length code were employed. In the worst case, for EUMETSAT images, which have approximately 150 rows, at least 1.73 bpp

Table 2: Context-based entropy analysis of IASI L0 data from EUMETSAT. Reported results in bpp (lower is better).

IASI L0 Product	Order-0	Order-1 Left	Order-1 Top-Left	Order-1 Top	Order-1 Top-Right	Order-1 One Previous	Order-1 Next to Previous	Order-2 Left and Top	Order-2 Two Previous	Order-3 Left and Top and One Previous	Order-3 Left and Two Previous	Order-3 Top and Two Previous
EUMETSAT 1	6.092	3.709	3.851	3.609	3.822	3.176	3.337	1.836	2.042	0.737	0.819	0.826
EUMETSAT 2	5.848	3.671	3.829	3.642	3.848	3.100	3.256	1.827	2.083	0.779	0.883	0.875
EUMETSAT 3	6.469	3.710	3.793	3.625	3.834	3.165	3.319	1.391	1.747	0.495	0.568	0.570
EUMETSAT 4	6.364	3.831	3.976	3.688	3.897	3.188	3.357	1.750	2.025	0.687	0.770	0.782
EUMETSAT 5	5.363	3.843	3.927	3.759	3.966	2.875	2.998	2.032	2.232	0.964	1.100	1.110
EUMETSAT 6	5.784	3.935	4.062	3.796	3.976	2.918	3.051	1.826	2.073	0.753	0.872	0.892
EUMETSAT 7	5.550	3.271	3.461	3.289	3.458	3.034	3.176	1.902	2.033	0.861	0.910	0.933
EUMETSAT 8	6.270	3.652	3.836	3.655	3.766	3.091	3.248	1.655	1.929	0.640	0.716	0.725
Average	5.967	3.702	3.841	3.632	3.820	3.068	3.217	1.777	2.020	0.739	0.829	0.839

Table 3: Context-based entropy analysis of IASI L0 data from CNES. Reported results in bpp (lower is better).

IASI L0 Product	Order-0	Order-1 Left	Order-1 Top-Left	Order-1 Top	Order-1 Top-Right	Order-1 One Previous	Order-1 Next To Previous	Order-2 Left and Top	Order-2 Two Previous	Order-3 Left and Top and One Previous	Order-3 Left and Two Previous	Order-3 Top and Two Previous
CNES 1	6.297	4.051	4.211	3.986	4.218	3.213	3.395	2.598	2.627	1.304	1.462	1.487
CNES 2	6.303	4.217	4.382	4.154	4.386	3.169	3.340	2.570	2.590	1.227	1.409	1.430
CNES 3	6.354	4.144	4.297	4.101	4.322	3.188	3.360	2.577	2.592	1.241	1.416	1.434
CNES 4	6.335	4.153	4.297	4.104	4.332	3.210	3.387	2.557	2.607	1.243	1.415	1.435
CNES 5	6.282	4.064	4.219	4.014	4.230	3.172	3.350	2.548	2.590	1.292	1.458	1.477
CNES 6	6.573	4.217	4.357	4.164	4.407	3.255	3.442	2.539	2.603	1.193	1.364	1.386
CNES 7	6.315	4.057	4.196	3.987	4.220	3.206	3.384	2.600	2.609	1.290	1.455	1.478
CNES 8	6.376	4.256	4.408	4.196	4.420	3.215	3.396	2.574	2.616	1.225	1.403	1.425
Average	6.354	4.144	4.295	4.088	4.316	3.203	3.381	2.570	2.604	1.251	1.422	1.444

could be spared; for CNES images, which have approximately 1500 rows, at least 1.62 bpp could be saved.

These gains could be higher if contextual models were used. When one pixel belonging to the same spatial component acts as context, on average, 4.45 bpp (images from EUMETSAT) and 3.98 bpp (images from CNES) might be saved. If spectral contexts, this is, the co-located pixel in a previous component, were used, it would be possible to spare, on average, 5.05 bpp in the case of images from EUMETSAT and 4.90 bpp for CNES. In the worst case, considering any order-1 context, 4.13 bpp and 3.78 bpp might be spared at least in images from EUMETSAT and CNES, respectively.

These results are further improved when order-2 conditional contexts are used. Taking as context the co-located pixels in the previous and the next to previous component allows us to spare, on average, 6.18 bpp in images from EUMETSAT and 5.59 bpp in images from CNES. The savings are greater when order-2 left and top pixel context is used. In this case, on average, 6.42 bpp and 5.63 bpp could be saved in images from EUMETSAT and CNES, respectively. In the worst

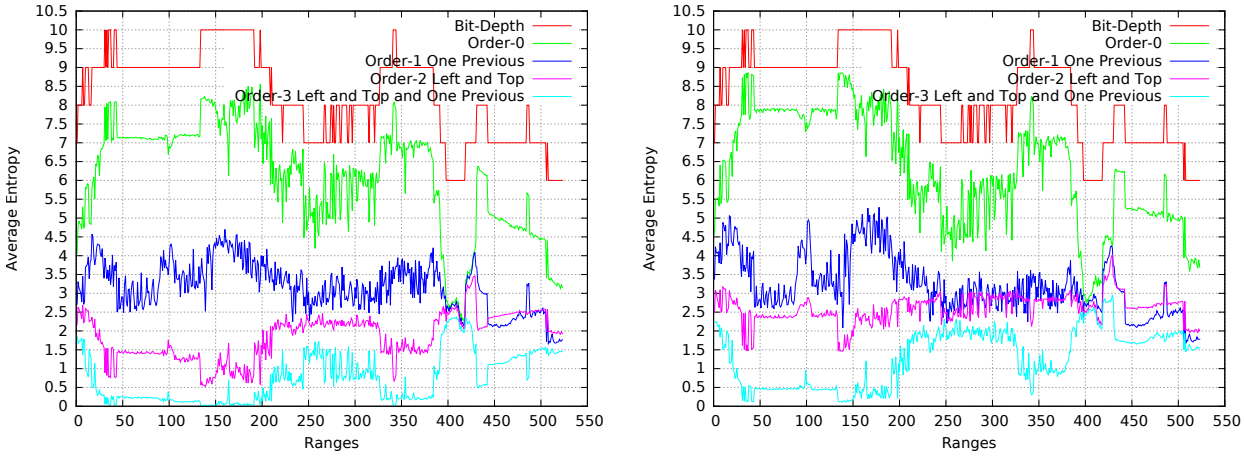

(a) EUMETSAT 1

(b) CNES 1

Figure 5: Average entropy analysis by ranges.

case, using any order-2 conditional context, 5.96 bpp might be saved in images from EUMETSAT and 5.57 bpp might be spared for CNES.

Nevertheless, the best results are obtained when order-3 conditional contexts are used. When one spatial neighboring pixel (the left or the top) and two spectral neighboring pixels (the co-located pixels in the previous and in the next to previous components) are used as context, it would be possible to save, on average, 7.36 bpp and 6.76 bit per pixel in images from EUMETSAT and CNES, respectively. When two spatial neighboring pixels (the left and the top) and one spectral neighboring pixel (the co-located pixel in the previous component) are used as context, on average, 7.46 bpp (images from EUMETSAT) and 6.94 bit per pixel (images from CNES) could be saved.

In general, using any contextual model improves the entropy results. Fig. 5a compares order-0, order-1 conditional entropy, order-2 conditional entropy and order-3 conditional entropy in the image EUMETSAT 1, along with the original bit-depth. Fig. 5b shows the same comparison for image CNES 1. To provide a clearer visual representation, only order-1 one previous component context (better on average), order-2 left and top context (better on average) and order-3 left and top and one previous component (better on average) are plotted. These plots show the average entropy per range, i.e., the X axis represents the 523 ranges in which a spectra is *divided*, and the Y axis represents the average entropy per range. Due to space constraints only two graphics are plotted. The results in the other images are almost identical to those shown here.

One can see how order-0 entropy already outperforms the current bit-depth in IASI L0 data. Comparing the different entropies, as expected, order-3 conditional entropy yields the best results in terms of bit rate in all ranges, followed by order-2, then order-1 and finally order-0. We also note that, for ranges between 398 and 431, order-0 is very similar to order-1, order-2 and order-3 conditional entropies.

Also, although in general order-2 left and top pixel context outperforms order-1 one previous component context in most ranges, this order-1 yields lower entropy for ranges between 430 and 523; in these ranges, spectral contexts yield better performance than spatial contexts (notice that we are comparing order-1 spectral against order-2 spatial).

For these same ranges, from 430 to 523, order-2 spectral context also outperforms order-2 spatial context. Obviously, order-2 spectral context is better than order-1 spectral context. For all the other ranges, order-2 spatial context is better than order-2 spectral context.

3 Compression of IASI L0 data

In this section we investigate the actual performance of different lossless coding techniques and standards on the two sets of IASI L0 data introduced earlier. The performance of the new CCSDS-123 standard, the M-CALIC technique, the well-known JPEG-LS and JPEG2000 standards for IASI L0 lossless data compression is tested.

The recently approved CCSDS-123 standard [7], [8] provides a competitive performance with a low computational cost for a large variety of multi-, hyper-, and ultra-spectral data. CCSDS-123 is a prediction-based coding technique specially designed to operate on-board of satellites. CCSDS-123 operates in a two-stage mode. In the first stage, an estimate of the current pixel is performed and used to compute a prediction residual. In the second stage, this prediction residual is first mapped to an integer and then encoded with a Golomb code.

M-CALIC [9] is a lossless and near-lossless compression technique for hyperspectral images based on context-based adaptive lossless image coding (CALIC) [10]. The algorithm uses a multiband spectral predictor, along with optimized model parameters and optimization thresholds. Correlation between bands by employing the two previous bands of the current line is exploited.

JPEG-LS [11] is a 2D low-complexity lossless and near-lossless compression technique that operates in a two-stage mode, modeling and encoding. It is specially designed to be simple and fast.

JPEG2000 [12], [13] is an international standard developed by the Joint Photographic Experts Group (JPEG). It is intended as the successor of JPEG in many of its application areas due to its superior compression performance.

Here, JPEG-LS and JPEG2000 are tested together with Pairwise Orthogonal Transform for Spectral Image Coding (POT) [14]. POT is based on the application of a divide-and-conquer strategy to the KLT [15], [16], where the resulting transform is a composition of smaller KLT transforms. In a full KLT, all components are decorrelated with each other, independently of how much energy they share. By contrast, the proposed POT has a structure that decorrelates parts with high shared energy while ignoring the other parts, as parts with low energies have a lower influence in the coding performance [14]. POT is used in the tests to perform a spectral transform before applying JPEG-LS or JPEG2000.

Although samples have an actual bit-depth precision from 6 to 10 bits, for storing purposes, each sample is stored in 2 bytes (16 bits), without sign. Each volume has 8359 bands, 60 columns and a variable number of rows. Images from EUMETSAT have between 110 and 196 rows. Images from CNES are larger, with between 1482 and 1528 rows.

As for the parameters employed in the experiments, CCSDS-123 lossless coding technique includes several user-specified configuration parameters. Here we resort to default parameters as suggested in [8]. In the last approach, once POT has been applied for spectral transform, JPEG2000 performs 2 levels of DWT spatial transform.

Table 4: Lossless compression performance of images from EUMETSAT. Reported results in compression ratio (higher is better) and bits per pixel (lower is better).

Compression ratios

IASI L0 Product	CCSDS-123	M-CALIC	POT+JPEG-LS	POT+JPEG2000
EUMETSAT 1	2.617	2.693	2.145	2.653
EUMETSAT 2	2.627	2.701	2.116	2.650
EUMETSAT 3	2.483	2.537	1.902	2.489
EUMETSAT 4	2.581	2.637	2.140	2.617
EUMETSAT 5	2.805	2.862	2.308	2.801
EUMETSAT 6	2.761	2.783	2.176	2.706
EUMETSAT 7	2.618	2.746	1.964	2.611
EUMETSAT 8	2.588	2.623	2.010	2.567
Average	2.635	2.697	2.095	2.636

Bits per pixel

IASI L0 Product	CCSDS-123	M-CALIC	POT+JPEG-LS	POT+JPEG2000
EUMETSAT 1	3.13	3.04	3.82	3.09
EUMETSAT 2	3.12	3.03	3.87	3.09
EUMETSAT 3	3.30	3.23	4.31	3.29
EUMETSAT 4	3.17	3.10	3.83	3.13
EUMETSAT 5	2.92	2.86	3.55	2.92
EUMETSAT 6	2.96	2.94	3.76	3.03
EUMETSAT 7	3.13	2.98	4.17	3.14
EUMETSAT 8	3.16	3.12	4.07	3.19
Average	3.11	3.03	3.92	3.11

Table 5: Lossless compression performance of images from CNES. Reported results in compression ratio (higher is better) and bits per pixel (lower is better).

Compression ratios

IASI L0 Product	CCSDS-123	M-CALIC	POT+JPEG-LS	POT+JPEG2000
CNES 1	2.839	2.874	2.614	2.858
CNES 2	2.846	2.858	2.596	2.834
CNES 3	2.857	2.873	2.597	2.847
CNES 4	2.840	2.859	2.585	2.832
CNES 5	2.843	2.871	2.605	2.857
CNES 6	2.835	2.834	2.569	2.819
CNES 7	2.843	2.883	2.605	2.852
CNES 8	2.832	2.823	2.574	2.812
Average	2.841	2.859	2.593	2.838

Bits per pixel

IASI L0 Product	CCSDS-123	M-CALIC	POT+JPEG-LS	POT+JPEG2000
CNES 1	2.88	2.85	3.13	2.86
CNES 2	2.88	2.86	3.15	2.89
CNES 3	2.87	2.85	3.15	2.88
CNES 4	2.88	2.86	3.17	2.89
CNES 5	2.88	2.85	3.14	2.87
CNES 6	2.89	2.89	3.19	2.90
CNES 7	2.88	2.84	3.14	2.87
CNES 8	2.89	2.90	3.18	2.91
Average	2.88	2.86	3.15	2.88

Table 4 and table 5 report the performance of CCSDS-123, M-CALIC, POT+JPEG-LS and POT+JPEG2000 for lossless compression of IASI L0 images.

The performance of CCSDS-123, M-CALIC and POT+JPEG2000 is very similar, while POT+JPEG-LS yields worse results. Although not reported here, applying a POT before JPEG-LS helps improve the performance of JPEG-LS by about 0.9 bpp.

On average, a compression ratio of 2.656:1 and 2.846:1 can be achieved for, respectively, EUMETSAT and CNES images using either CCSDS-123, M-CALIC or POT+JPEG2000. Compression ratio has been computed considering the length of the original image bit-stream and the length of the compressed codestream.

Related to entropy results reported earlier in Tables 2 and 3, order-2 entropy analysis indicated that, on average, images from EUMETSAT and CNES might be coded using about 1.89 and 2.58 bpp, respectively. Here we see that CCSDS-123, M-CALIC and POT+JPEG2000 allows to compress these images using, on average, 3.08 and 2.87 bpp, respectively, which is very close to the theoretical optimal compression when order-2 context are used –at least for CNES images, which have a larger row size and may better represent the average performance–.

CCSDS-123 is specially designed to operate on-board satellites. It has low computational requirements and acceptable

performance. Transmission rate for IASI Level 0 data could be further decreased, or even some more data could be transmitted at the original transmission rate if CCSDS-123 were considered as a candidate for on-board lossless compression of IASI L0 data. M-CALIC and POT+JPEG2000 achieve also good performance, but their computational requirements are higher.

A brief discussion follows on the potential of integrating CCSDS-123 in the IASI on-board processing chain. The IASI instrument has a data production rate of 45 Mbit/s, at varying sample bit depths, and it has a total power consumption of 210 W [17]. The *fast lossless* compressor, on which the CCSDS-123 standard is based, has been implemented by Aranki et. al in XILINX VIRTEX IV and VIRTEX V FPGAs [18], [19], [20]. The authors report an implementation capable of operating at 40 Msample/s with a power consumption of 700mW, which seem to fit the requirements of the IASI instrument.

4 Conclusion

The Infrared Atmospheric Sounder Interferometer (IASI) is a key element of the payload on the Metop series of European meteorological polar-orbiting satellites (EUMETSAT). The instrument provides atmospheric spectra to derive temperature and humidity profiles to the scientific and meteorological communities. The data production rate in the instrument is 45 Megabits/s while the transmission rate allocated to IASI measurements is 1.5 Megabits/s. Consequently, a significant part of the IASI data processing is performed on board the instrument before transmitting data to reception stations.

In this paper we analyzed the potential of entropy coding in IASI L0 data. A theoretical analysis of order-0 entropy, order-1 conditional entropy, order-2 conditional entropy and order-3 conditional entropy, where conditional entropies assess both the spectral and the spatial joint information, was performed. This analysis yielded that at least 1.6 bits per pixel (bpp) might be saved if a simple variable-length code were employed. The best results were obtained when order-3 contextual models were used, allowing to spare at least 6.7 bpp.

We also investigated the performance of different lossless compression techniques on IASI L0 data. The recent CCSDS Recommended Standard for Lossless Multispectral & Hyperspectral image compression (CCSDS-123), the JPEG-LS and JPEG2000 standards and the M-CALIC coding technique were evaluated. Experimental results suggested that, on average, a compression ratio of 2.6:1 could be achieved for images with, approximately, 150 rows. The performance was even better for larger images (1500 rows, approximately), reaching a compression ratio of 2.8:1.

Given that CCSDS-123 is a competitive and efficient coding technique whose hardware implementation is amenable to satellite probes, a particularly interesting point to consider in the future could be the potential of CCSDS-123 on IASI raw data, i.e., even before the on-board processing chain has taken place, as the on-board processing introduces loss because a quantisation is carried out. It might be worth investigating whether CCSDS-123 lossless compression could be applied on original IASI raw data, thus enabling transmission of data that has not gone through any irreversible processing.

5 Acknowledgments

This work was supported in part by FEDER, the Spanish Government (MINECO), the Catalan Government, and the Centre National d'Études Spatiales (CNES), under grants TIN2012-38102-C03-03 and 2014SGR-691.

An earlier version of this work was presented at the ESA CNES On-Board Payload Data Compression Workshop 2014.

We thank the reviewers for their comments, which have helped to improve the quality of the paper.

References

[1] G. Chalon, F. Cayla, and D. Diebel, "IASI: An advanced sounder for operational meteorology," *International Astronautical Congress (IAF) 52 nd*, Procedings, 2001.

[2] CNES, "Dossier de définition des algorithmes IASI," REF. IA-DF-0000-2006-CNE, 2009.

[3] CNES, "Spécification Technique de Besoin du logiciel opérationnel IASI," REF. IA-SB-2100-9462-CNE, 2006.

[4] EUMETSAT, "Metop Design - IASI," 2014. [Online]. Available: http://www.eumetsat.int/website/home/Satellites/CurrentSatellites/Metop/MetopDesign/IASI/index.html

[5] EUMETSAT, "IASI Measurement and Verification Data," REF. IA-ID-1000-6477-AER, 2010.

[6] B. Tournier, D. Blumstein, F. Cayla, and G. Chalon, "IASI level 0 and 1 processing algorithms description," *ISTCXII Conference*, Proceedings, 2002.

[7] Consultative Committee for Space Data Systems (CCSDS), *Lossless Multispectral & Hyperspectral Image Compression CCSDS 123.0-B-1*, ser. Blue Book. CCSDS, May 2012. [Online]. Available: http://public.ccsds.org/publications/archive/123x0b1ec1.pdf

[8] E. Augé, J. Sánchez, A. Kiely, I. Blanes, and J. Serra-Sagristà, "Performance impact of parameter tuning on the CCSDS-123 lossless multi- and hyperspectral image compression standard," *Journal of Applied Remote Sensing*, vol. 7, no. 1, p. 074594, August 2013.

[9] E. Magli, G. Olmo, and E. Quacchio, "Optimized onboard lossless and near-lossless compression of hyperspectral data using CALIC," *Geoscience and Remote Sensing Letters, IEEE*, vol. 1, no. 1, pp. 21–25, 2004.

[10] X. Wu and N. Memon, "Context-based, adaptive, lossless image coding," *Communications, IEEE Transactions on*, vol. 45, no. 4, pp. 437–444, 1997.

[11] M. Weinberger, G. Seroussi, and G. Sapiro, "The LOCO-I lossless image compression algorithm: principles and standardization into JPEG-LS," *Image Processing, IEEE Transactions on*, vol. 9, no. 8, pp. 1309–1324, 2000.

[12] D.S.Taubman and M. Marcellin, *JPEG2000 Image Compression Fundamentals, Standards and Practice: Image Compression Fundamentals, Standards, and Practice*. Springer, 2002.

[13] JPEG-Committee, "Standard jpeg2000," 2014. [Online]. Available: http://www.jpeg.org/jpeg2000

[14] I. Blanes and J. Serra-Sagristà, "Pairwise orthogonal transform for spectral image coding," *Geoscience and Remote Sensing, IEEE Transactions*, vol. 49, no. 3, pp. 961–972, 2011.

[15] J. A. Saghri, S. Schroeder, and A. Tescher, "An adaptive two-stage KLT scheme for spectral decorrelation in hyperspectral bandwidth compression," *SPIE Optical Engineering+Applications. International Society for Optics and Photonics*, pp. 744 313–744 313–12, 2009.

[16] R. Dony, (editors: K.R.Rao, and P.C.Yip), *The transform and data compression handbook, Chapter 1. Karhunen-Loeve Transform*. CRC Press, 2001.

[17] ESA, "Meteorological operational satellite program of europe," https://directory.eoportal.org/web/eoportal/satellite-missions/m/metop.

[18] N. Aranki, D. Keymeulen, M. Klimesh, and A. Bakhshi, "Fast and adaptive lossless on-board hyperspectral data compression system for space applications," *IEEE Aerospace Conference*, 2009.

[19] ——, "Hardware implementation of lossless adaptive and scalable hyperspectral data compression for space," *NASA/ESA Conference on Adaptive Hardware and Systems*, p. 315322, 2009.

[20] N. A. nad D. Keymeulen, A. Bakhshi, J. Kang, M. Klimesh, and A. Kiely, "FPGA provides speedy data compression for hyperspectral imagery," *Xilinx Newsletter*, 2012.